Configuration Tracking for Continuum Manipulators With Coupled Tendon Drive

David B. Camarillo, *Member, IEEE*, Christopher R. Carlson, and J. Kenneth Salisbury, *Member, IEEE*

***Abstract*—Robotic control of flexible devices can enhance and simplify many medical procedures. We present a method for controlling a tendon-driven continuum manipulator by means of specifying the shape configuration. The basis for control is a linear beam configuration model that transforms beam configuration to tendon displacement by modeling internal loads of the compliant system. An essential aspect of this model is the inclusion of both the mechanical and geometrical coupling among serial articulating sections. Important capabilities of this model are the general forward kinematics and the decoupled inverse kinematics that allow for independent control of multiple sections. Tracking results are presented for a cardiac catheter with two articulating sections.**

***Index Terms*—Cable drive, continuum robot, flexible arm, medical robot.**

I. Introduction

FLEXIBLE manipulators are found in a variety of fields, from medical to aerospace, where there is a requirement for long thin instruments. In the medical field, the growing popularity of minimally invasive treatments has spurred the development of many new and increasingly complex catheter like instruments [1]–[3]. This complexity can be effectively managed with robotic control that provides more dexterous and stable manipulation at reduced scales [4]–[6].

In medical applications, building very small instruments to conform to anatomy in often required. To make fabrication feasible at these scales, relatively simple designs are most attractive. Therefore, flexible elements with embedded transmission lines for remote actuation can be used to avoid miniature joints and pulleys. This construction has worked well in the past for simple instruments, such as a steerable catheter that has one tendon to articulate the tip. However, for higher degree-of-freedom (DOF) controlled motion, we would like to embed multiple tendons terminated various locations along the length of the catheter to create multiple bending sections (such as that shown Fig. 1). If no further measures are taken to mechanically isolate these sections, we observe the following behavior: 1) *tendon load coupling* of distal tendon forces back onto more proximal sections and 2) geometrical *tendon path coupling* of proximal articulations to distal tendon displacements. To achieve independent control of multiple-section continuum manipulators, we must model both varieties of coupling. Therefore, the primary contribution of this paper is the first model to include both the tendon load and tendon path coupling effects.

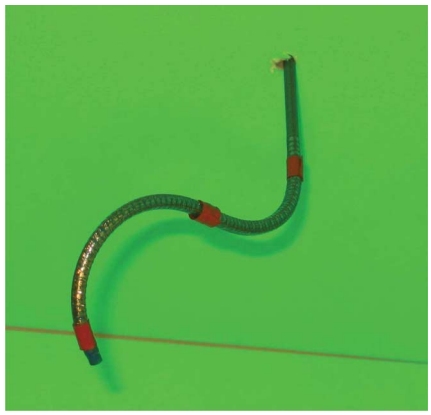

Fig. 1. Catheter with two articulating sections and two tendons per section arranged antagonistically from distal to proximal.

Tendon actuation is not the only means for controlling minimally invasive medical instruments. Sears and Dupont [7], as well as Webster *et al.* [8], have used beam mechanics to understand and control a series of preshaped, concentric tube instruments that may be extended and rotated within one another to form various configurations. One motivating factor for constructions based on preshaped tubes is ease of miniaturization. With tendon actuation, miniaturization involves not only smaller moment arms for bending but reduced bending stiffness as well; therefore, miniaturization may be achievable here as well. While analyses of preshaped tubes have some similarity to this paper, tendon actuation has its own set of behaviors, including these coupling effects that are the focus of this paper.

Hirose investigated the tendon load coupling of a high-DOF tendon-driven arm for increasing load-carrying capacity [9]. He modeled the tendon load coupling of distal tendons on proximal joints to allow for joint torque control. His design consisted of rigid links and discrete joints with pulleys to route the tendons along the planar arm. In the case of a continuum manipulator, we are not constrained to using pulleys at joints; therefore, we can route tendons multidimensionally to accomplish 3-D articulation. Moreover, the axial mode of our catheter is compliant; therefore, we must model the axial force coupling in addition to

Manuscript received July 1, 2008; revised December 23, 2008. First published June 5, 2009; current version published July 31, 2009. This paper was recommended for publication by Associate Editor T. Murphey and Editor K. Lynch upon evaluation of the reviewers' comments. This work was supported in part by the Stanford Bio-X Graduate Fellowship and by Hansen Medical, Inc.

D. B. Camarillo was with the Biorobotics Laboratory, Stanford University, Stanford, CA 94305 USA. He is now with Hansen Medical, Inc., Mountain View, CA 94043 USA (e-mail: dbcamarillo@stanfordalumni.org).

C. R. Carlson is with Hansen Medical, Inc., Mountain View, CA 94043 USA (e-mail: ccarlson@hansenmedical.com).

J. K. Salisbury is with the Biorobotics Laboratory, Stanford University, Stanford, CA 94305 USA (e-mail: jks@robotics.stanford.edu).

Color versions of one or more of the figures in this paper are available online at http://ieeexplore.ieee.org.

Digital Object Identifier 10.1109/TRO.2009.2022426

the moments. While our analysis is quite different, the model is similar to that of Hirose with respect to tendon load coupling.

A novel tendon path decoupling scheme was proposed by Jones and Walker [10], which they termed "tangle/untangle." Their solution consisted of two separate algorithms used in either the forward or inverse kinematics. The algorithms were written for manipulators with three cables per section offset at $120/m^\circ$ intervals for each of m sections. These algorithms accurately couple and decouple the tendon length paths of a purely kinematic manipulator. However, for a manipulator with compliance in the axial mode and tendons, the loads must also be modeled because the deformations would affect the kinematic parameters in the algorithm. For example, unknown tendon stretch would prevent accurate calculation of the most proximal section's configuration, thereby propagating forward to all subsequent distal sections. In this case, the "untangle" would not be suitable as a stand-alone module in the forward kinematics. Therefore, we model the tendon path coupling as a function of load, which can be used simultaneously with the tendon load coupling for the forward and inverse kinematics of a catheter.

The need for a complete decoupling framework has been alluded to in [11]–[14] and is our principal aim in this paper. We begin from the basis of a mechanics model for a single section presented in [14] and [15]. We now carry out a full analysis of the 3-D mechanics in Section II and the Appendix, including experiments to validate the modeled response in Section IV. From this basis of 3-D single-section mechanics, we extend the model to include multiple sections in Section III that was briefly summarized in [16]. The tendon load coupling and tendon path coupling naturally fit into the framework of our existing model. The result is the complete beam configuration model, which provides a general forward and inverse kinematic mapping from tendon displacement to beam configuration. The inverse kinematics are then used in the experiments of Section V to achieve independent control of the two articulating sections for the catheter in Fig. 1.

II. 3-D Mechanics of a Single Section

We initially presented a 3-D extension [15] of our 2-D beam configuration model [14] that relates tendon displacement to beam configuration. Now, we substantiate the 3-D model through static beam analysis and experiments of a single isolated continuum section. The output of the mechanics analysis is a constitutive equation relating the mechanical response of beam strain (or configuration) due to tendon force. In order to associate tendon displacement with beam configuration, we combine the constitutive equation with conservation of strain yielding the beam configuration model. This beam configuration model is linear and may readily be inverted on its own or could be used as a module for achieving higher level goals, such as task-space control.

A. 3-D Statics

Our goal in analyzing beam statics is to arrive at the two fundamental equations that govern the 3-D behavior of a tendon actuated beam, as shown in Fig. 2. The first equation relates the loading characteristics of the compliant elements in the system, and the second relates their displacements. The single tendon pictured in gray in Fig. 2 is terminated at the distal end and passes freely through lumens (on the perimeter of the cross section) back through the proximal end where it may be actuated by displacement. This embedded tendon (labeled j in cross section) may apply a force T_j that results in its own displacement and a moment on the beam. The displacement and moment are related to the location of the tendon $[d_{xj}, d_{zj}]$ in the beam cross section.

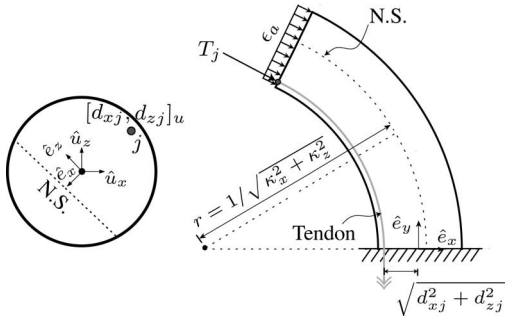

Fig. 2. Beam illustrates single articulating section with a single tendon terminated at the distal end. Circle is a cross-section view in fixed u frame. The location of tendon j is given with $[d_{xj}, d_{zj}]_u$. When tendon j is actuated with force T_j, the resulting neutral surface (N.S.), as well as the articulation e frame, is illustrated. Beam is illustrated in the $\hat{e}_x$–$\hat{e}_y$ bend plane. Bend radius r is shown in terms of curvatures κ_x and κ_z in the u frame. Axial strain ϵ_a is also shown, which occurs along the longitudinal axis of the manipulator.

Tendon loading results in constant-curvature beam bending in a single plane with no torsion (demonstrated in the Appendix). The deformation of the beam under load can then be parameterized by only three variables: curvature about two axes κ_x and κ_z of the neutral surface, as well as axial compression ϵ_a. Note that the magnitude of the neutral surface's curvature is reduced from the centroid's curvature only by the axial compression percentage. Alternatively, an angular representation of the distal tip articulation could be used which avoids making the distinction between the centroid and the neutral surface. Curvature is used here since a moment required to bend a beam is dictated by curvature. In practice, this assumed state of deformation captured by only κ_x, κ_z, and ϵ_a is valid for our millimeter-scale catheters constructed of superelastic composites since linear elasticity dominates other effects, such as gravity, inertia, and friction (see [14] for further comments on neutral surface and loading assumptions, and [15] for 3-D data). With this assumed state of deformation shown in Fig. 2, we may proceed toward the two fundamental equations relating beam configuration, tendon force, and tendon displacement.

The configuration of a tendon actuated beam may be expressed in terms of the applied tendon loading. The Appendix analyzes the mechanical response of a beam under tendon loading. Balancing the internal loading from deformation and the external loading due to tendon actuation yields the constitutive equation, which is the first principle

beam equation

$$\begin{bmatrix} K_b & 0 & 0 \\ 0 & K_b & 0 \\ 0 & 0 & K_a \end{bmatrix} \begin{bmatrix} \kappa_x \\ \kappa_z \\ \epsilon_a \end{bmatrix} = \begin{bmatrix} d_{z0} & d_{z1} & \dots & d_{zn} \\ -d_{x0} & -d_{x1} & \dots & -d_{xn} \\ 1 & 1 & \dots & 1 \end{bmatrix} \begin{bmatrix} T_0 \\ T_1 \\ \vdots \\ T_n \end{bmatrix} \quad (1)$$

and in matrix form, it is written as

$$\mathbf{K}_m\, \mathbf{q} = \mathbf{D}\, \boldsymbol{\tau}. \quad (2)$$

The configuration space parameterization of the manipulator is then described with curvature and axial compression in $\mathbf{q}$. The bending and axial beam stiffnesses, K_b (in newtons per square millimeter) and K_a (in newtons), are contained in $\mathbf{K}_m$. On the left side of (2), the stiffness of the manipulator is multiplied by the configuration (beam strain), which results in the internal manipulator loading. This loading must be accomplished by external tendon actuation; therefore, the right side of (2) cross multiplies the tendon tensions $\boldsymbol{\tau}$ by their moment arms in $\mathbf{D}$. This constitutive equation captures the linear elastic mechanical response of the manipulator in equilibrium.

This static equilibrium condition in (2) must be satisfied with the appropriate $\boldsymbol{\tau}$ to realize a desired configuration $\mathbf{q}$. It should be noted that this equation has no tendon displacement information, which is the traditional method of control. Next, we will introduce tendon displacement as part of the model; therefore, control may be achieved with motor position control. However, this intermediate step of modeling forces is crucial in understanding controllability in tendon drive with compliant tendons and/or an axially compliant manipulator. For example, configurations with high articulation angle may require significant force and, therefore, tendon displacement due to axial compression of the manipulator and tendon stretch. Another example of the need for force information is the situation where the desired configuration is zero axial strain. Analyzing the required forces would indicate that negative tendon tension is required, even though it is not physically possible. A pure kinematic model can suffice if a manipulator is axially rigid and tendon strain is small in comparison to bending strain, but accounting for the compliant mechanics can improve performance in many situations.

In order to translate mechanical response into tendon displacements, we must link tendon tension to tendon displacement. Tendon displacement $\mathbf{y}$ is composed of bending ($\boldsymbol{\epsilon}_{bx}$, $\boldsymbol{\epsilon}_{bz}$) and axial ($\boldsymbol{\epsilon}_a$) strain of the beam along the tendon path, as well as tendon strain ($\boldsymbol{\epsilon}_t$)

$$\begin{aligned} \mathbf{y} &= l_0\, (\boldsymbol{\epsilon}_{bx} + \boldsymbol{\epsilon}_{bz} + \boldsymbol{\epsilon}_a) + l_t\, \boldsymbol{\epsilon}_t \\ &= \mathbf{D}^T\, \mathbf{L}_0\, \mathbf{q} + \mathbf{L}_t\, \mathbf{K}_t^{-1}\, \boldsymbol{\tau}. \end{aligned} \quad (3)$$

We refer to (3) as conservation of strain, where $\mathbf{L}_0 = \mathrm{diag}(l_0)$ has the undeformed section length, $\mathbf{L}_t = \mathrm{diag}(l_t)$ has the undeformed tendon lengths, and $\mathbf{K}_t^{-1} = \mathrm{diag}(1/K_t)$ is the tendon compliance (in inverse newton). Note the presence of the transpose of the tendon moment arm matrix $\mathbf{D}^T$, indicating the force/displacement duality. This duality is particularly important in the coupling of multiple sections, which will be described later.

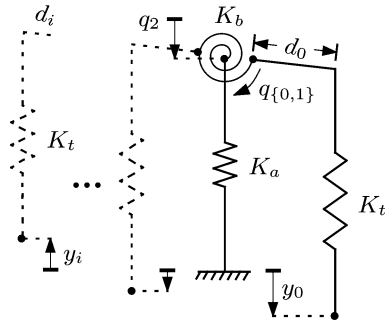

Fig. 3. Planar spring model for the tendon–manipulator system. Rotational spring is bending mode, central grounded spring is manipulator's axial mode, and peripheral springs are tendons. The system is shown for a single tendon (solid on right), but it can also be used to model n tendons (dashed on left).

The constitutive and conservation of strain equations together describe a lumped-parameter model consisting of a system of springs, as illustrated in Fig. 3. The constitutive equation (2) is Hooke's law for the rotational and center grounded springs, which represent the beam's bending ($q_{\{0,1\}}$) and axial (q_2) modes, respectively. Conservation of strain (3) allows for the peripheral tendons to be added to the system, whereby their displacement must include the beam's deformation as well as their own stretch. This spring system is very useful in building intuition for the behavior of a manipulator. For example, the existence of a solution for the forward kinematics from tendon displacement to beam configuration is obvious in that displacing the tendon springs will visually result in some rotational equilibrium.

B. Beam Configuration Kinematic Model

Here, we develop the kinematic model and discuss the forward and inverse paths for under- and overactuated systems while considering tendon slack. Fig. 3 allows one to visualize the relationship between tendon displacement and manipulator configuration. We formalize this relationship by combining (2) and (3) to solve for the beam configuration model

$$\mathbf{y} = \mathbf{C}_m\, \boldsymbol{\tau} \quad (4)$$

where the compliance matrix is given as

$$\mathbf{C}_m = \mathbf{D}^T\, \mathbf{L}_0\, \mathbf{K}_m^{-1}\, \mathbf{D} + \mathbf{L}_t\, \mathbf{K}_t^{-1}$$

leading to

$$\mathbf{q} = \mathbf{A}\, \mathbf{y} \quad (5)$$

where the forward kinematics transformation matrix is given as

$$\mathbf{A} = \mathbf{K}_m^{-1}\, \mathbf{D}\, \mathbf{C}_m^{-1}.$$

Equation (4) describes the input–output relationship between tendon tension and displacement. $\mathbf{C}_m$ is square and invertible since any set of tendon displacements always has an associated set of tensions (ignoring slack for now). $\mathbf{K}_m$ is invertible as well since it is diagonal. Therefore, the forward kinematics (5) work

by multiplying the known tendon displacements $\mathbf{y}$ by $\mathbf{C}_m^{-1}$ to determine tendon tensions, then by $\mathbf{D}$ to calculate the associated internal beam loads, and finally by $\mathbf{K}_m^{-1}$ to give beam strains or configuration. For a feasible solution to exist via tendon actuation, we must also require that

$$\boldsymbol{\tau} \geq \mathbf{0}. \tag{6}$$

The beam configuration model (5) is run in the forward direction for any manipulator by simple matrix multiplication. It may also be run in the inverse direction using standard closed-form solutions, such as least squares or minimum norm, depending on actuator arrangement. However, these simple methods do not account for slack and therefore should be used with caution. In situations where slack may occur, we must ensure positive tendon tension (6) by more advanced optimization techniques.

C. Forward Kinematics With Slack

For arbitrary tendon displacements in Fig. 3, a configuration will always be reached, yet not necessarily with positive tendon tension. We physically assume that tendons provide only tension; therefore, negative tension (i.e., tendon compression) invalidates the model. Negative tension indicates that a tendon has gone slack. Therefore, the model could be recovered by relaxing the displacement constraint and adding a zero tension constraint for slack tendons. However, the location of zero tension is not obvious since backing out a spring that was in negative tension causes all other loads as well as the configuration to change. If we estimate that a tendon has gone slack, we can model tendon slack by introducing the estimated tendon displacement $\hat{\mathbf{y}}$ and the slack displacement $\boldsymbol{\delta}$ in

$$\mathbf{y} = \hat{\mathbf{y}} + \boldsymbol{\delta}. \tag{7}$$

Here, the estimated tendon displacement $\hat{\mathbf{y}}$ would come from encoder readings, for example, but the effective tendon displacement $\mathbf{y}$ corresponds to the tendon path with zero tension. The difference is the slack, which is backlash that contributes no actuation effort in deforming the manipulator. The elements of the slack vector $\boldsymbol{\delta}$ would be zero for all tendons that are in tension and positive for any slack tendons.

In many cases, we assume that slack will not occur from *a priori* knowledge of the design of the inverse kinematic controller [14]. In this case, running the forward kinematics (5) directly is correct. If the presence of slack is in question [can be checked by inverting (4)], a correct solution to the forward kinematics requires determining the extent of slack through an optimization problem

$$\begin{aligned} \underset{\boldsymbol{\delta}}{\text{minimize}} \quad & \boldsymbol{\delta}^T \, \mathbf{C}_m^{-1} \, (\hat{\mathbf{y}} + \boldsymbol{\delta}) \\ \text{subject to} \quad & \mathbf{C}_m^{-1} \, (\hat{\mathbf{y}} + \boldsymbol{\delta}) \geq \mathbf{0} \\ & \boldsymbol{\delta} \geq \mathbf{0}. \end{aligned} \tag{8}$$

Minimizing the objective function in (8) to zero means that slack tendons will contribute no force. This is because $\mathbf{C}_m^{-1}(\hat{\mathbf{y}} + \boldsymbol{\delta})$ is the vector of all tendon tensions (slack elements are zero), and multiplying by the elements of the slack vector $\boldsymbol{\delta}$ will zero all nonslack elements. When slack tendons contribute no force, we know that a feasible solution has been reached.

The inequality constraints in (8) ensure that no tendons can impart negative compressive force and that slack can only be a positive displacement. $\mathbf{C}_m^{-1}(\hat{\mathbf{y}} + \boldsymbol{\delta}) \geq \mathbf{0}$ is the usual positive tendon tension constraint. Slack displacement can only be in the direction of tendon compression (otherwise tension would develop); therefore, we must also constrain $\boldsymbol{\delta} \geq \mathbf{0}$. Physically, we know that there is a single feasible solution for any set of tendon displacements. Therefore, (8) may be solved using nonlinear convex optimization, and the objective function will be minimized to zero.

The solution for $\boldsymbol{\delta}$ corresponds to the physical slack displacement in the tendons and can be used in (7) to compute the effective tendon displacements (without slack) for the model. These adjusted displacements allow for valid use of the model since no negative forces will exist. The forward kinematics (5) can then be solved for the manipulator configuration in the presence of slack. Alternatively, an inverse kinematics method that does not account for slack can be used, and then, any slack can be estimated with (7) and then servoed out as a second step. In either case, it is important to avoid slack both for maintaining control authority and for the practical risks of buckling damage (depending on tendon material) or falling off of a drive pulley.

D. Inverse Kinematics

Selecting an appropriate method for inverting (5) depends upon tendon arrangement. For example, if the manipulator is overactuated, we can choose an inverse of $\mathbf{D}$ such as the minimum norm for relieving tendon tensions ($\mathbf{K}_m$ and $\mathbf{C}_m$ are square and invertible so that $\mathbf{A}^\dagger = \mathbf{C}_m \mathbf{D}^\dagger \mathbf{K}_m$). However, other constrained optimization techniques may be required to protect against slack tendons since the minimum-norm example does not guarantee a feasible solution with respect to positive tension [14]. In the case of underactuation, a different method would be required. A general formulation for the inverse kinematics using convex optimization is possible, but here, we focus on a single method relying upon *a priori* knowledge of tendon arrangement and configuration inputs.

Assuming we are using an underactuated manipulator, we can specify relative weightings for the configurations of most interest on the diagonals of $\mathbf{W}$. Given underactuation, visualizing input configurations that are only possible with positive tendon tension is within reason. Therefore, we operate within this set of input configurations and ignore slack tendons. Ignoring slack allows us to compute the inverse kinematics using the Moore–Penrose pseudoinverse

$$\mathbf{A}^\dagger = \text{pinv}(\mathbf{W}\,\mathbf{A})\,\mathbf{W}. \tag{9}$$

This solution minimizes the square error on the weighted version of the configuration vector. This should achieve the configuration variables of interest as specified in $\mathbf{W}$ while ignoring the remaining variables with zero entries.

III. Decoupling Multiple Serial Sections

In order to accomplish higher DOF tasks, a continuum manipulator may be constructed with multiple serial sections. The theory describing an isolated section can be extended to multiple

sections but must account for coupling among sections. There are two principle mechanisms of coupling: 1) *tendon load coupling* of distal tendon loads on proximal sections and 2) *tendon path coupling* of proximal articulation paths on distal tendons. Hirose [9] has investigated tendon load coupling while Jones and Walker [10] have investigated tendon path coupling. Here, we present a unified formulation for considering both of these important phenomena simultaneously in our beam configuration model.

A. Tendon Load Coupling

The catheter pictured in Fig. 1 has two articulating sections. To articulate the distal section, we must apply actuation force on the distal tendons, which, in turn, impose a load on the proximal section. If this load is not counteracted by the proximal tendons, the proximal section will articulate as well. It is not sufficient to hold the initial position of the proximal tendons fixed because the proximal section may compress or its tendons may stretch due to the distal load. Therefore, it is necessary to model this tendon load coupling and account for it if we are to achieve decoupled control.

From the 3-D analysis of a single section in the Appendix, we found that tendon actuation leads to a constant moment and compressive force on any cross section (with no torsion). For the multiple-section case, we found that loading of a tendon terminated on the mth distal-most section of a manipulator couples back on any given proximal section exactly as if that distal tendon were terminated on that proximal section. This distal to proximal tendon load coupling can be captured in the constitutive equation (2) with the upper triangular tendon coupling matrix

$$\mathbf{D} = \begin{bmatrix} \mathbf{D}_0 & \mathbf{D}_1 & \cdots & \mathbf{D}_m \\ & \mathbf{D}_1 & \cdots & \vdots \\ & & \ddots & \vdots \\ \mathbf{0} & & & \mathbf{D}_m \end{bmatrix} \tag{10}$$

where each $\mathbf{D}_i$ contains the tendon moment arms for the ith section.

This tendon coupling matrix for a multisection manipulator can be used in the original constitutive matrix equation (2) by augmenting the other vectors and matrices. The configuration is now described by triples of curvatures and axial compression repeated for each section along $\mathbf{q}$ from proximal to distal. The tendon tensions are grouped by section along the length of $\boldsymbol{\tau}$, also from proximal to distal. $\mathbf{K}_m$ is now block diagonal with its single-section diagonal components. For a manipulator with n tendons and m sections, the dimensions in the constitutive equation are $\mathbf{q} \in \mathbb{R}^{3m}$, $\boldsymbol{\tau} \in \mathbb{R}^n$, $\mathbf{K}_m \in \mathbb{R}^{3m \times 3m}$, and $\mathbf{D} \in \mathbb{R}^{3m \times n}$. Therefore, (2) describes the mechanical response of an m-section manipulator.

B. Tendon Path Coupling

When a proximal section is articulated, any tendons terminated at a more distal section will also change the path. If it is desired to control the distal configuration simultaneously, we must know and account for the amount of change due to proximal bending and compression. However, proximal configuration is not sufficient information for decoupling the distal section if it has another more distal section imparting loads back. Therefore, we develop a model for proximal to distal tendon path coupling that can be combined with the distal to proximal mechanical load coupling. Together, they form the basis for independent control of proximal and distal sections in our beam configuration model.

The conservation of strain equation (3) can model the tendon path coupling by augmenting the matrices from the single-section case. The transpose of the tendon coupling matrix (10) $\mathbf{D}^T$ captures the kinematic coupling from configuration to tendon path. $\mathbf{D}^T$ acts to sum the bending and compressive strains in the manipulator from all sections proximal to a given tendon. Therefore, this one matrix $\mathbf{D}$ serves the purpose of describing both the tendon load coupling and tendon path coupling since they are the dual of each other.

To complete the extension to multiple sections, we must consider the effects of tendon stretch on the right-hand side of (3). Tendon stretch is a function of the unstrained tendon length, and further out distal sections must have longer tendons. The total length of a set of tendons terminated at a given section is the sum of all previously proximal section lengths. This is captured in diagonal blocks within the tendon length matrix

$$\mathbf{L}_t = \begin{bmatrix} \operatorname{diag}(l_0) & & & \mathbf{0} \\ & \operatorname{diag}(l_0 + l_1) & & \\ & & \ddots & \\ \mathbf{0} & & & \operatorname{diag}\left(\sum_{i=0}^{m} l_i\right) \end{bmatrix} \in \mathbb{R}^{n \times n}.$$

The tendon stiffness matrix $\mathbf{K}_t \in \mathbb{R}^{n \times n}$ and section length matrix $\mathbf{L}_0 \in \mathbb{R}^{3m \times 3m}$ are simply block diagonal with components of their individual sections. The augmented conservation of strain equation now models the tendon path coupling.

Combining the conservation of strain with the constitutive equation as before yields the same form of the beam configuration model (5). The forward kinematics matrix $\mathbf{A}$ now contains the complete mechanics including both mechanisms of coupling. The generalized inverse of $\mathbf{A}$ can decouple the sections when there is sufficient actuation authority to provide independent control of the multiple sections.

IV. Mechanics Experiments

We carry out experiments to verify the mechanics from the previous sections and identify the model parameters. To verify the form of the constitutive equations from our analyses, we observe the coupling from tendon load to bending configurations. Given confidence in the underlying mechanics, we must then identify the model parameters to use the inverse kinematics in control.

A. Experimental Setup

The continuum manipulator we use is the catheter in Fig. 1. This catheter consists of a long 700-mm proximal portion that would travel through the patient's venous system and two shorter 60-mm distal sections for articulating in the chambers of the

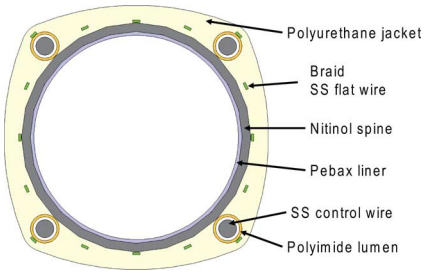

Fig. 4. Catheter constituent materials in cross-sectional view.

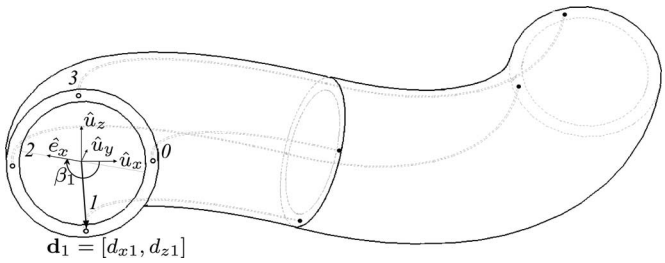

Fig. 5. Schematic of catheter with two articulating sections and four numbered tendons. View is from proximal to distal such that the tendons would continue out of the page through the proximal shaft. Distally terminated tendons 2 and 3 articulate distal section. Proximally terminated tendons 0 and 1 support and articulate proximal section resulting in articulation plane β_1. A vector indicating location of tendon 1 $\mathbf{d}_1$ is displayed.

heart. The catheter is a composite with a superelastic Nickel Titanium (NiTi) spine laminated with plastics about a steel braid to constrain the tendons (see cross section in Fig. 4). The tendons themselves pass through low-friction polyimide lumens. The spine is a NiTi tube that has been laser cut into a series of flexure hinges in alternating directions. The overall catheter is 4.0 mm in outer diameter and has an open working channel. For these experiments, a steel mandrel is used to stiffen the proximal section from any bending that would otherwise be supported by a patient's anatomy.

To minimize experimental complexity while achieving proof of concept, only four total tendons are embedded. Their locations are illustrated in Fig. 5, where two tendons are terminated on the proximal articulating section (0 and 1) and two on the distal section (2 and 3). All distal tendons can be thought of as usable for controlling a proximal section owing to tendon path coupling. Therefore, the proximal section in Fig. 5 may be fully articulated in all directions with four tendons. The distal section, on the other hand, may articulate only in the negative x-direction and positive z-direction and is coupled to the proximal section. These actuation capabilities may be a limiting factor in configuration space but, depending on the application, may be fully sufficient for task-space operation of the distal tip over a significant volume. In any case, this basic experimental setup was chosen to allow for antagonistic bending of the proximal and distal sections that demonstrates coupling with interesting shapes.

The catheter is actuated by the robot in Fig. 6(a), which displaces the tendons via spools. The spools are mounted on bearing-supported torque-sensing shafts to measure tendon tension. The shafts are driven by the robot's dc motor encoder servos that are powered by high-bandwidth current amplifiers for proportional–derivative (PD) position control. Tendon displacement control is explored instead of force control since it is simpler from a hardware perspective. In addition, under position control, configuration is less affected by unmodeled disturbances, such as friction or external contact, given a geared down drive train.

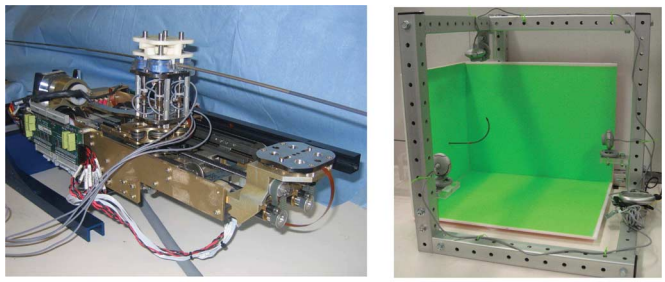

(a) (b)

Fig. 6. Experimental setup. (a) Robot for actuation with torque-sensing drive shafts. (b) Vision system used to measure catheter articulation.

TABLE I
THREE-SECTION MANIPULATOR PARAMETERS

Section	K_a; K_b	K_t	$[d_x, d_z]_j$	l_0	l_t
0	8,890; 1e7	-	-	700	-
1	530; 530	4,450	$[1.98,-0.21]_0$ $[0.01,-2.00]_1$	64	764
2	530; 530	4,450	$[-1.94,0.48]_2$ $[-0.15,1.99]_3$	61	825

Data measurements for the beam articulation are achieved using the vision system shown in Fig. 6(b) [15]. This system extracts a 3-D point cloud of the manipulator shape and can distinguish the marked colored marker bands that indicate section transitions. The data are then fit with a curve and is registered to the catheter frame using the proximal most marker band. If necessary, the curve can also be fit to a circle to approximate the catheter shape. In this case, the length assigned to a circular arc is the length of the associated curve between markers. The origin of the circle is registered to the position and orientation of the appropriate proximal marker for a given section. In these experiments, the circle approximation is useful for extracting the plane of articulation, as will be presented shortly.

Prior to carrying out any mechanics experiments, the specific locations of the tendons should be known. This information can come from the design, but catheter manufacturing and fixturing induce some variability. An accurate estimate of tendon locations is desirable because the model is sensitive to angular errors as they are amplified by the articulation length. Therefore, we experimentally identify the tendon locations parameterized by their polar coordinates of magnitude and angle. The magnitude is the distance from centroid to tendon in the cross-sectional plane, which is measured as half the catheter diameter. The angle of a tendon is measured with the camera system given by the plane of articulation under single tendon actuation. The identified locations for the two proximal and two distal tendons are listed in Table I and correspond approximately to Fig. 5.

B. Bend Coupling Data

The beam configuration model relies on the mechanical response described by the constitutive equation (2), and therefore, we should verify this experimentally. From the experiments in [14], the linear elastic relationship between tendon tension and beam bending (as well as axial compression) was confirmed using the single-section planar case. In 3-D, there is now coupling of the tendon tensions to bending about two axes for a single section and $2m$ axes for multiple sections. For the single-section case, 3-D data for the measured and modeled catheter curves are presented in [15]. In general, coupling may be quantified concisely by comparing the angle of bend moment from $\mathbf{D}\boldsymbol{\tau}$ to the measured bend plane. In this way, we will see that distally accumulated moments set a given section's bend plane. The definition of bend plane β_i of the ith section is

$$\beta_i := \tan^{-1}\left(\frac{\kappa_{zi}}{\kappa_{xi}}\right) + \frac{\pi}{2}.$$

The constitutive equation indicates that these curvatures are caused by the corresponding moments in $\mathbf{D}\boldsymbol{\tau}$. Therefore, the angle of these moments about y in the x–z plane should correlate 1:1 with bend plane. We set up an experiment to measure $\boldsymbol{\tau}$ and the bend planes β_i over a range of articulations for comparison with the modeled response.

Given the relationships between proximal and distal antagonistic tendons, we articulate the proximal section through multiple articulations with initial bend planes of $\beta_1 = 180°$–$270°$, while at each proximal articulation, the distal section is exercised through multiple articulations in bend planes from $\beta_2 = 0°$–$90°$. The bend plane ranges were selected based on the 90° angular offset tendon arrangement. The total articulation angle for each data point was near 90° of distal tip flexion to get a well-conditioned measurement for the bend plane. These articulations were achieved by displacing two tendons at a time in flexion while visually monitoring the catheter. Data for the tendon tensions as well as the bend plane angles were recorded. The articulation data are plotted in Fig. 7 as the measured bend plane over the calculated moment angle. The moment angle $\angle M$ is from the polar coordinate transformation of the Cartesian vector of the first two elements of $\mathbf{D}\boldsymbol{\tau}$ for a given section.

Fig. 7 shows the proximal and distal bend planes as a function of the proximal, distal, and cumulative moment angles. Since, in the modeled response, the angle of the coupled back moment is exactly the bend plane, we plot this prediction as the solid line of slope 1.0. On the top row, we can see that the distal bend plane correlates with the distal moment angle, as predicted, and not with the cumulative moment angle. This seems obvious that proximal forces do not affect distal articulation; however, it emphasizes the point that distal articulation is governed directly by forces and not tendon kinematics. On the bottom row, the distal articulation plane correlates with the cumulative moment angle, as predicted. In addition, the proximal bend plane spans almost 140°, even though its tendons are only approximately 90° apart, which is due to distal coupling. For all of these articulations, no torsion was observed, and the data follow the model response; therefore, the coupled mechanics in the constitutive equation is verified.

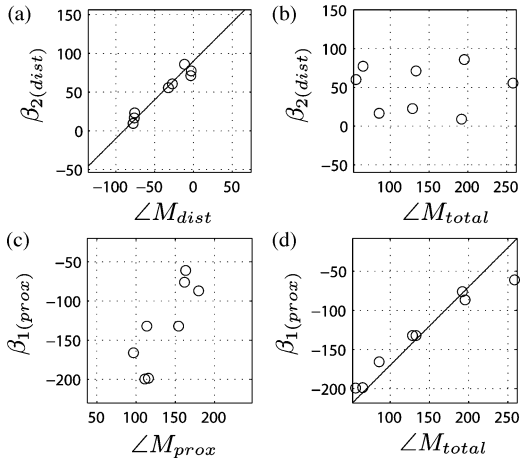

Fig. 7. Moment angle to bend plane coupling for two articulating sections with data points as circles and modeled response as lines. Distal bend plane is shown as a function of (a) distal tendon moment angle and (b) cumulative tendon moment angle. Proximal bend plane is shown as a function of (c) proximal tendon moment angle and (d) cumulative tendon moment angle.

C. Parameter Identification

Before achieving control, we must identify the model parameters, and we present one such method here. The parameters to be identified are the manipulator and tendon stiffnesses as well as the manipulator's kinematic parameters. All length measurements were taken by means of calipers or a yardstick. The bending articulations were measured with the vision system (although vision system could also be used for distal length measurements).

As mentioned, the tendon locations in $\mathbf{D}$ were determined from the catheter cross-sectional radius and articulation planes. The tendon stiffness was determined by external testing of tensile strain using an Instron machine. The axial stiffness for the manipulator's most proximal section was determined by the tension sensors and measured linear shrink. For the distal sections, the shrink was measured using a coaxial tube down the working channel, which would protrude and become exposed during catheter articulation.

The manipulator parameters are listed in Table I. All the lengths are in millimeters, axial stiffness in newtons, bending stiffness in newtons per square millimeter, and j is the tendon number. The most proximal section 0 is given a very high bend stiffness since it does not articulate and has no tendons. The stiffness parameters for the two articulating sections 1 and 2 are assumed to be equal since they are of the same construction.

V. Configuration Tracking

To demonstrate the utility of this beam configuration model, we drive the catheter from Fig. 1 to track commanded configuration inputs. This requires using the inverse kinematics to generate an input to the robot's tendon position controller, which, in turn, actuates the catheter. First, we command the catheter

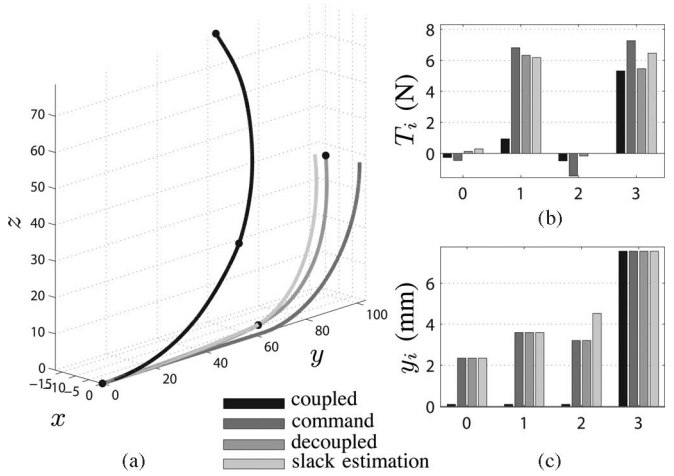

Fig. 8. Distal articulations where we plot (a) configurations including the command, the vision measured articulation data with and without coupling (spheres indicating colored marker bands), as well as the slack-estimated configuration. (b) Estimated and measured tendon tensions for the articulations (where 0,1 are proximal and 2,3 are distal tendons). (c) Tendon displacements for articulations.

through a simple distal articulation to highlight successful decoupling and compare it with the alternative. Next, we present a more complicated configuration command that is accurately reached. Finally, we demonstrate coordinated tracking control of multiple sections by achieving a pure roll motion.

Configuration tracking is achieved using the inverse kinematics and tendon position control. For the present three-section manipulator where $\mathbf{A} \in \mathbb{R}^{9\times 4}$, there are nine configuration variables and only four tendons; therefore, the system is underactuated. This was accounted for in the design since the proximal section is largely rigid in bending, and we do not intend to control the axial compressions for these experiments. Therefore, before inverting the forward kinematics, we first multiply by a weighting matrix $\mathbf{W} = \text{diag}(0,0,0,1,1,0,1,1,0)$, indicating that we will only penalize errors on the two pairs of distal curvature commands.

The inverse kinematic solution (9) is used to compute the tendon commands for the configuration where the proximal articulating section remains straight and the distal section flexes through 90° in the z-direction. The "decoupled" curve in Fig. 8(a) plots the vision measured shape, where the spheres indicate section transitions demarcated by the colored markers. For comparison, the "command" given to the inverse kinematics is plotted adjacent. Note that the catheter nearly achieves the straight proximal section with the articulated distal section as commanded but with a slight bias in the $-x$ direction due to slack. We quantify slack by solving (8) with $\hat{\mathbf{y}}$ from the inverse kinematics to yield the slack vector $\boldsymbol{\delta}$. $\hat{\mathbf{y}} + \boldsymbol{\delta}$ is then a physically realistic estimate of the effective tendon displacement without slack. This displacement is then run through the forward kinematics, and the output configuration "slack estimation" is plotted. Therefore, we originally chose a configuration that could not be tracked given the tendon arrangement (tendon 3 is slightly to the left of top dead center), but the slack estimation accurately predicts the measured configuration.

To understand the mechanics associated with this distal articulation, the "decoupled" tendon forces are recorded during the experiment and plotted in Fig. 8(b). The antagonistic proximal and distal tendons 1 and 3 balance out in force to prevent the proximal section from articulating. Since the command was in the z-direction, the tendons 0 and 2 along the x-axis bear no load. Although we expect little tendon load, small tension measurements are a warning sign of unobservable slack; therefore, we should examine the estimated tensions from the model.

The simulated forces for this distal articulation are computed by inverting (4) given $\mathbf{y}$ for both the cases of unbounded actuation and slack-limited actuation. The case of unbounded actuation from the inverse kinematics "command" is given in Fig. 8(b) and shows some negative load in the simulation. This occurs because the distal articulating tendon 3 here has a slight component in the $-x$ direction, and there are no distal tendons with positive x. In this situation, the inverse kinematics (9) attempts to push with tendon 2 to achieve the configuration. Therefore, pure z articulation is not feasible as it is on the edge of our configuration workspace. However, our model can still reflect this physical situation by estimating the slack. The "slack estimation" is also shown in Fig. 8(b) and reflects that no tendon can impart negative loads and closely matches the "decoupled" measured tensions.

In Fig. 8(c), we plot the tendon displacement "command" from our inverse kinematics. Proximal tendons 0 and 1 must displace to account for proximal compression. Tendon 1 antagonistically supports the proximal section from bending; therefore, it must displace additionally to account for its own stretch. Distal tendon 2 bears little load; therefore, it must only displace to account for proximal and distal compressions. Although tendon 3 bears equal load to tendon 1, it must also cover the distal bend path; therefore, it displaces the most. The originally computed "command" from the inverse kinematics was the source of the applied tendon displacements for the "decoupled" experiment; therefore, these two sets of displacements are equivalent. However, the forward kinematics with "slack estimation" computed a slack displacement, which can be seen on tendon 2.

For a purely geometric model (no modeled compliance) aiming to achieve a similar configuration, traction of only the single distal tendon would be required. Therefore, we apply this "coupled" displacement [given in Fig. 8(c)] for comparison. The resulting "coupled" catheter articulation is shown in Fig. 8(a), and the coupling into a proximal bend is apparent. As distal traction force is applied, the proximal section begins to compress, thus allowing room to move against the proximal tendons and, therefore, bending from coupled back load. For this experiment, the antagonistic proximal tendon 1 was slightly taught (and therefore stretching), but in general, this depends on the location of the neutral surface [15].

To demonstrate the performance of the model with a more complicated shape, Fig. 9(a) has both sections bending in different planes and with different curvatures. The configuration tracking is adequate with a tip-to-tip error of 7 mm over the 125-mm articulating beam length. In addition, the measured and simulated tensions match well in Fig. 9(b). Since all estimated tensions are greater than zero, slack compensation was

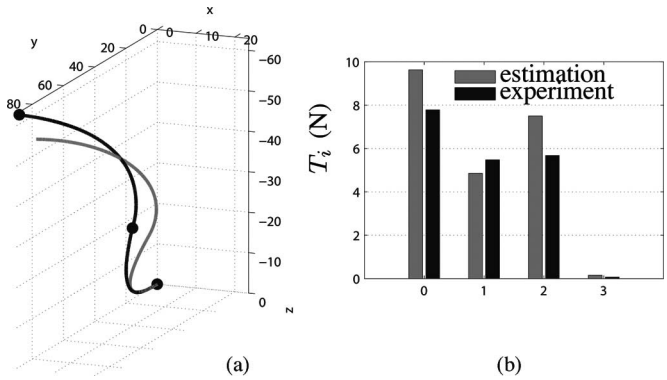

Fig. 9. Decoupled control of distal and proximal articulating sections. (a) Configuration plot of vision experimental data compared with estimation. (b) Tension experimental data compared with estimation.

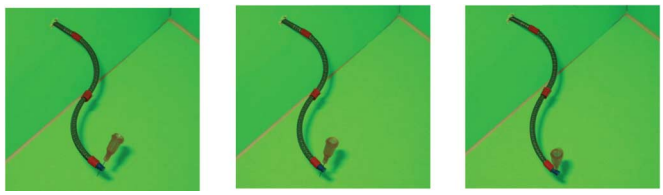

Fig. 10. Pure roll about a fixed axis is achieved by rotating catheter shaft in one direction and rotating commands of articulating sections in the opposite directions. Rotation may be seen by pin orientation (and shadow) of the leftmost image progressing through the rightmost image.

not necessary. Errors in tension are possibly due to insufficient pretension (or creep) since we cannot be aggressive without antagonistic actuation on a single section. Generally, it is helpful to slightly preload all tendons, but this is not possible without antagonistic actuation on each section. In addition, the stiffness estimations will have error due to noisy compression measurements. For configuration, errors may arise from hysteresis where the catheter may not have returned to entire straight configuration before pretension. In addition, the section transition has stiff portion, which is not presently modeled.

Coordinated motion of the two sections is demonstrated by achieving a pure roll motion about the catheter axis. This is accomplished by issuing articulation commands of constant-curvature magnitude but rotating in direction. The rate of rotation is equal for the two sections, but opposite that of the shaft which is rolled by the robot. In Fig. 10, we can see that over this time series from left to right, the catheter position holds while it rolls, as evidenced by the pin marker. For future surgical applications, this maneuver is particularly important as it is required to drive a needle when suturing.

VI. Conclusion

This paper presented a method for achieving independent control of multiple sections of a tendon-driven continuum manipulator. This was accomplished by unifying the tendon load coupling and tendon path coupling in our beam configuration model. A general method for the forward kinematics of this model was presented, which accounts for slack-limited tendon actuation. One method for inverse kinematics was presented for underactuated manipulators by weighting configuration parameters of interest. We presented configuration-tracking data for multiple articulations along with simulation to illustrate the working principles and verify model performance.

Appendix

Equilibrium in a Cantilever Beam With Embedded Tendons

Our goal is to show that tendon actuation is consistent with an assumed 3-D beam deflection and that the mechanical response is linear. We will show that this result holds for n tendons and m serially coupled articulating sections. This linear response of beam deformation due to tendon loading is the basis for the constitutive equation (2).

Imagine that the proximal section in Fig. 5 is a single isolated continuum section supported as a cantilever beam. We begin by assuming the beam is uniformly compressing and bending in a single articulation plane with no torsion. With uniform deformation on all cross sections in the absence of shear (2 DOF) and torsion (1 DOF), there are only three configuration state variables to describe the entire deformation (i.e., bending strains κ_x, κ_z and compressive strain ϵ_a). The internal loading in this situation is described in the u frame by multiplying these strains by their stiffnesses

$$[F_x,\ F_y,\ F_z]^T = [0,\ K_a\,\epsilon_a,\ 0]^T \tag{11}$$

$$[M_x,\ M_y,\ M_z]^T = [K_b\,\kappa_x,\ 0,\ K_b\,\kappa_z]^T. \tag{12}$$

Having specified the internal loading and geometry, we examine the external loading from tendon actuation to show consistency with the assumed geometry in a linear form.

Fig. 5 illustrates the u frame that is fixed in the material of the proximal end of a section. The moving e frame is also in this proximal end but rotates about $\hat{u}_y$ by β to define the plane of articulation. Assume a single arbitrary tendon is terminated on the distal end of this beam, and its location is described in the u frame as $\mathbf{d} = [d_x, 0, d_z]$. The $\hat{e}_x$–$\hat{e}_y$ planar projection of this scenario is illustrated in Fig. 11 as a free-body diagram. A third coordinate frame b is illustrated as a rotation of e about $\hat{e}_z$ to describe the articulation plane at the distal end. Note that this free-body diagram can be used to calculate reaction loads on any beam cross section and, therefore, applies to all cross sections.

There are two forces from the tendon tension T that we must consider: the termination force $\mathbf{F}_t$ and the equivalent contact force $\mathbf{F}_{\text{eq}}$ (equivalent to distributed load $\mathbf{w}(s)$ caused by tendon curvature κ_t). Both of these forces are parallel to the bend plane. Given Euler rotation matrices $\mathbf{R}_y(\beta)$, $\mathbf{R}_z(\phi)$, we can calculate the effect of these two loads on the proximal cross section in the u frame

$$\mathbf{F}_{\text{eq}} = \mathbf{R}_y(\beta) \int_{\phi=0}^{\phi=\phi_b} \mathbf{R}_z(\phi)\,[-T\,\kappa_t,\ 0,\ 0]^T\,\mathrm{d}s$$

$$\mathbf{F}_t = \mathbf{R}_y(\beta)\,\mathbf{R}_z(\phi_b)\,[0,\ -T,\ 0]^T.$$

These forces impart an associated moment on the proximal cross section; therefore, we must specify their tendon moment arms

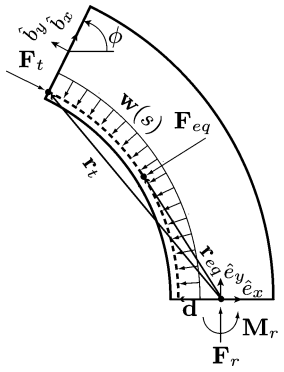

Fig. 11. Free-body diagram for an isolated continuum section viewed in articulation plane. Dashed line is single tendon that imparts termination force and contact force.

as well

$$\mathbf{r_t} = \mathbf{R}_y(\beta)\left[\frac{(\cos\phi_b - 1)}{\kappa_t},\ \sin\frac{\phi_b}{\kappa_t},\ 0\right]^T + \mathbf{d}$$

$$\mathbf{r_{eq}} = \mathbf{R}_y(\beta)\left[\frac{(\cos(\phi_b/2) - 1)}{\kappa_t},\ \sin\frac{\phi_b/2}{\kappa_t},\ 0\right]^T + \mathbf{d}.$$

Given these forces and their moment arms, we can calculate the total external load on the cross section

$$\begin{aligned}\mathbf{F}_r &= \mathbf{F}_{\mathrm{eq}} + \mathbf{F}_t \\ &= [0,\ -T,\ 0]^T \end{aligned} \tag{13}$$

and the associated moment

$$\begin{aligned}\mathbf{M}_r &= \mathbf{r}_t \times \mathbf{F}_t + \mathbf{r}_{\mathrm{eq}} \times \mathbf{F}_{\mathrm{eq}} \\ &= [d_z\, T,\ 0,\ -d_x\, T]^T. \end{aligned} \tag{14}$$

To satisfy equilibrium, these external loads (13) and (14) must equal the internal loads (11) and (12) from material strain over the entire beam. Since our analysis applies to any cross section, it is apparent that an equilibrium will exist and depends linearly upon the tendon tension T. This balance of external and internal loads results in the constitutive equation (2).

We have shown that the external loading of tendon actuation can satisfy the required internal loading of axial compression with torsion-free, constant-curvature bending in a single plane. Since (13) and (14) are linear in T, by superposition, the same form holds for n tendons by summing additional moments and forces. A given set of tendon tensions will be able to satisfy the same geometrical constraints with a resulting pair of curvatures and an axial compression. Therefore, we have shown that the constitutive equation (2) may describe manipulators with multiple tendons, such as the proximal section of Fig. 5, or even redundantly actuated manipulators.

Finally, this analysis can apply to multiple serial section manipulators, including the whole manipulator of Fig. 5. For the single section we examined in Fig. 11, all cross sections experience the same loading. Therefore, if this single section were the distal most (mth) section of a manipulator, its proximal end would have the same loading as its distal end where its tendons were terminated. This means that tendon termination loading of the mth section couples back onto the $(m-1)$th section identically, where the two sections are joined. Any additional tendons terminated at the distal end of the $(m-1)$th section simply add in by superposition, as before. This argument recurses for more proximal sections, meaning that the load on a given section is determined by all tendons terminated distally as if they were terminated at the present section. Coupling of tendon loads in this linear fashion allows for the constitutive equation (2) to describe multiple-section loading simply with an augmentation (10).

The uncovered mechanics here support our earlier work [15], including the aspect of torsion-free articulation. The torsion-free result confirms the correction in [17] of the error in [18] by Walker *et al.* However, the analysis here suggests that the reason for torsion-free articulation is the absence of torsional load rather than backbone design.

ACKNOWLEDGMENT

The authors thank A. Kowshik, K. Loewke, and G. Stahler for their work on the catheter, vision system, and tension sensors.

REFERENCES

[1] A. Kapoor, K. Xu, W. Wei, N. Simaan, and R. Taylor, "Telemanipulation of snake-like robots for minimally invasive surgery of the upper airway," in *Proc. MICCAI Med. Robot. Workshop*, 2006, pp. 17–25.

[2] K. Ikuta, T. Hasegawa, and S. Daifu, "Hyper redundant miniature manipulator "hyper finger" for remote minimally invasive surgery in deep area," in *Proc. IEEE ICRA*, 2003, pp. 1098–1102.

[3] A. Al-Ahmad, "Utilizing robotic catheter control technology for EP procedures," *EP Lab Dig.*, vol. 7, no. 8, pp. 20–22, 2007.

[4] D. Camarillo, T. Krummel, and J. Salisbury, "Robotic technology in surgery: Past, present, and future," *Amer. J. Surg.*, vol. 188, no. 4A, pp. 2S–15S, 2004.

[5] R. Satava, "Emerging technologies for surgery in the 21st century," *Arch. Surg.*, vol. 134, no. 11, pp. 1197–1202, 1999.

[6] R. Taylor, "Robots as surgical assistants: Where we are, wither we are tending, and how to get there," in *Proc. AIME*, 1997, pp. 3–11.

[7] P. Sears and P. Dupont, "Inverse kinematics of concentric tube steerable needles," in *Proc. IEEE ICRA*, 2007, pp. 1887–1892.

[8] R. Webster, III, J. M. Romano, and N. J. Cowan, "Mechanics of precurved-tube continuum robots," *IEEE Trans. Robot.*, vol. 25, no. 1, pp. 67–78, Feb. 2009.

[9] S. Hirose, *Biologically Inspired Robots, Snake-Like Locomotors and Manipulators*, 1st ed. Oxford, U.K.: Oxford Univ. Press, 1993.

[10] B. Jones and I. Walker, "Practical kinematics for real-time implementation of continuum robots," *IEEE Trans. Robot.*, vol. 22, no. 6, pp. 1087–1099, Dec. 2006.

[11] M. Hannan and I. Walker, "Real-time shape estimation for continuum robots using vision," *Robotica*, vol. 23, no. 5, pp. 645–651, 2005.

[12] V. Chitrakaran, A. Behal, D. Dawson, and I. Waker, "Setpoint regulation of continuum robots using fixed camera," *Robotica*, vol. 25, no. 5, pp. 581–586, 2007.

[13] K. Xu and N. Simman, "An investigation of the intrinsic force sensing capabilities of continuum robots," *IEEE Trans. Robot.*, vol. 24, no. 3, pp. 576–87, Jun. 2008.

[14] D. Camarillo, C. Milne, C. Carlson, M. Zinn, and J. Salisbury, "Mechanics modeling of tendon driven continuum manipulators," *IEEE Trans. Robot.*, vol. 24, no. 6, pp. 1262–1273, Dec. 2008.

[15] D. Camarillo, K. Loewke, C. Carlson, and J. Salisbury, "Vision based 3-D shape sensing of flexible manipulators," in *Proc. IEEE ICRA*, 2008, pp. 2940–2947.

[16] D. Camarillo, C. Carlson, and J. Salisbury, "Task-space control for a continuum manipulator," in *Springer Tracts in Advanced Robotics*, Berlin, Germany: Springer-Verlag, 2009, vol. 54, pp. 271–280.

[17] B. Jones and I. Walker, "Kinematics for multisection continuum robots," *IEEE Trans. Robot.*, vol. 22, no. 1, pp. 43–55, Feb. 2006.

[18] M. Hannan and I. Walker, "Kinematics and the implementation of an elephant's trunk manipulator and other continuum style robots," *J. Robot. Syst.*, vol. 20, no. 2, pp. 45–63, 2003.

David B. Camarillo (M'08) received the B.S.E. degree in mechanical and aerospace engineering from Princeton University, Princeton, NJ, and the M.S. and Ph.D. degrees in mechanical engineering from Stanford University, Stanford, CA.

From 2003 to 2004, he was with Intuitive Surgical, Inc., where he was involved in a National Institutes of Health-funded robotic endoscope project. Since 2005, he has been a Senior Controls Engineer with Hansen Medical, Inc., Mountain View, CA, where he is involved in developing a flexible robotic surgery system. His current research interests include modeling and control of mechatronic systems, particularly for biomedical applications.

Christopher R. Carlson received the Ph.D. degree in mechanical engineering from the Dynamic Design Laboratory, Stanford University, Stanford, CA, in 2003.

He is currently the Senior Director of Engineering with Hansen Medical, Inc., Mountain View, CA. His current research interests include modeling, identification, and control of dynamic systems with classical as well as computational tools, and land vehicles and medical robots.

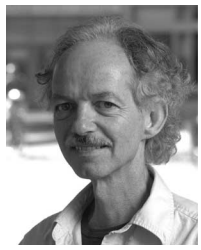

J. Kenneth Salisbury (M'08) received the Ph.D. degree in mechanical engineering from Stanford University, Stanford, CA, in 1982.

He is currently a Professor of computer science, surgery, and mechanical engineering at Stanford University, Stanford, CA. His current research interests include hands as manifested in robots, human–robot interactions, and computer haptics. He is also engaged in research on addressing fundamental issues in medical simulation and the creation of miniature surgical instruments. He was a Scientific Advisor with Intuitive Surgical, Inc., and a Technical Advisor with Robotic Ventures, Inc. He holds more than 25 patents. He has contributed to several commercially viable robots, including Intuitive Surgical's da Vinci Surgical Robot, SensAble Technologies' PHaNTOM Haptic Interface, Barrett Technology's Whole Arm Manipulator, the Salisbury Hand, and the forthcoming Personal Robot 1.

Prof. Salisbury was a member of the National Science Foundation's Advisory Council for Robotics and Human Augmentation.